REPORT DOCUMENTATION PAGE

Form Approved OMB NO. 0704-0188

1. REPORT DATE (DD-MM-YYYY)	2. REPORT TYPE	3. DATES COVERED (From - To)
22-01-2015	Conference Proceeding	-

4. TITLE AND SUBTITLE	5a. CONTRACT NUMBER
PERFORMANCE OF A SPLITTERED TRANSONIC ROTOR WITH SEVERAL TIP CLEARANCES	
	5b. GRANT NUMBER
	ARO MI-PR--
	5c. PROGRAM ELEMENT NUMBER
	611102

6. AUTHORS	5d. PROJECT NUMBER
Anthony J. Gannon , Garth V. Hobson, Mark G. Turner, Wolfgang Sanz	
	5e. TASK NUMBER
	5f. WORK UNIT NUMBER

7. PERFORMING ORGANIZATION NAMES AND ADDRESSES	8. PERFORMING ORGANIZATION REPORT NUMBER
Naval Postgraduate School (NPS-Monterey) 14,973.00 1 University Circle Monterey, CA 93943 -5000	

9. SPONSORING/MONITORING AGENCY NAME(S) AND ADDRESS (ES)	10. SPONSOR/MONITOR'S ACRONYM(S) ARO
U.S. Army Research Office P.O. Box 12211 Research Triangle Park, NC 27709-2211	11. SPONSOR/MONITOR'S REPORT NUMBER(S) 60039-EG.4

12. DISTRIBUTION AVAILIBILITY STATEMENT

Approved for public release; distribution is unlimited.

13. SUPPLEMENTARY NOTES

The views, opinions and/or findings contained in this report are those of the author(s) and should not contrued as an official Department of the Army position, policy or decision, unless so designated by other documentation.

14. ABSTRACT

The effect of increasing the tip-gap size on the performance of a splittered transonic rotor is presented. Tip clearance has a large influence on the performance and efficiency of compressors and fans during operation. In a gas turbine engine the ratio of tip-gap to blade height or span usually increases in the direction of flow. The front stages usually have a smaller ratio of tip-gap to blade height than the aft core stages. In addition the front stages are usually operating in the transonic regime while the rear stages operate sub-sonically.
In order to be representative of these differing flow regimes the results of a range of tests at varying tip-gaps and

15. SUBJECT TERMS

Transonic Rotor, Tip Clearance, Splittered rotor

16. SECURITY CLASSIFICATION OF:			17. LIMITATION OF ABSTRACT	15. NUMBER OF PAGES	19a. NAME OF RESPONSIBLE PERSON
a. REPORT	b. ABSTRACT	c. THIS PAGE			Garth Hobson
UU	UU	UU	UU		19b. TELEPHONE NUMBER 831-656-2888

Standard Form 298 (Rev 8/98)
Prescribed by ANSI Std. Z39.18

Report Title

PERFORMANCE OF A SPLITTERED TRANSONIC ROTOR WITH SEVERAL TIP CLEARANCES

ABSTRACT

The effect of increasing the tip-gap size on the performance of a splittered transonic rotor is presented. Tip clearance has a large influence on the performance and efficiency of compressors and fans during operation. In a gas turbine engine the ratio of tip-gap to blade height or span usually increases in the direction of flow. The front stages usually have a smaller ratio of tip-gap to blade height than the aft core stages. In addition the front stages are usually operating in the transonic regime while the rear stages operate sub-sonically.

In order to be representative of these differing flow regimes the results of a range of tests at varying tip-gaps and speeds from subsonic to transonic are presented. A highly loaded transonic axial splittered rotor is used as the test article in this study. Three experiments with cold tip gaps of 0.53 [mm], 0.76 [mm] and 0.99 [mm] are presented. Each experiment was run at six tip-Mach numbers ranging from Mach 0.72 to Mach 1.2 each over a full speed-line from choked to stalling conditions. Exit temperature and pressure profiles at the rotor exit are presented along with performance maps of pressure ratio and efficiency. Significant differences in performance in terms of pressure ratio, efficiency and operating range due to the tip-gap increase were observed and are presented.

The full mechanical geometry is available upon request to provide an open test case to evaluate simulation codes. This includes the cold-shape, the cavity between the rotor and stationary exit and the mounting bolts and geometry. The manufacturing steps in the preparation of the material and methods used to form the abradable material used over the rotor are presented. In addition the inlet conditions taking into account the effect of relative humidity on gas properties are presented. The complete data set of experimental results is also available electronically.

Conference Name: ASME Turbo Expo 2015

Conference Date: June 15, 2015

GT2015-43799

PERFORMANCE OF A SPLITTERED TRANSONIC ROTOR WITH SEVERAL TIP CLEARANCES.

**Anthony J. Gannon &
Garth V. Hobson**

Turbopropulsion Laboratory
Naval Postgraduate School
700 Dyer Rd, Monterey
CA 93940, USA

Mark G. Turner

Aerospace Engineering
University of Cincinnati
2600 Clifton Ave, Cincinnati OH
45220, USA

Wolfgang Sanz

Inst. f. Thermal Turbomachinery
and Machine Dynamics
Graz University of Technology
8010 Graz, Austria

ABSTRACT

The effect of increasing the tip-gap size on the performance of a splittered transonic rotor is presented. Tip clearance has a large influence on the performance and efficiency of compressors and fans during operation. In a gas turbine engine the ratio of tip-gap to blade height or span usually increases in the direction of flow. The front stages usually have a smaller ratio of tip-gap to blade height than the aft core stages. In addition the front stages are usually operating in the transonic regime while the rear stages operate sub-sonically.

In order to be representative of these differing flow regimes the results of a range of tests at varying tip-gaps and speeds from subsonic to transonic are presented. A highly loaded transonic axial splittered rotor is used as the test article in this study. Three experiments with cold tip gaps of 0.53 [mm], 0.76 [mm] and 0.99 [mm] are presented. Each experiment was run at six tip-Mach numbers ranging from Mach 0.72 to Mach 1.2 each over a full speed-line from choked to stalling conditions. Exit temperature and pressure profiles at the rotor exit are presented along with performance maps of pressure ratio and efficiency. Significant differences in performance in terms of pressure ratio, efficiency and operating range due to the tip-gap increase were observed and are presented.

The full mechanical geometry is available upon request to provide an open test case to evaluate simulation codes. This includes the cold-shape, the cavity between the rotor and stationary exit and the mounting bolts and geometry. The manufacturing steps in the preparation of the material and methods used to form the abradable material used over the rotor are presented. In addition the inlet conditions taking into account the effect of relative humidity on gas properties are presented. The complete data set of experimental results is also available electronically.

INTRODUCTION

Tip clearance effects in compressors and fans have a dramatic impact on performance, and have been a topic of interest for many years. Cumpsty in his book [1] has done an excellent job of presenting these effects drawing from a presentation by Freeman [2] at a VKI lecture. Wisler describes the effects in his lecture notes [3]. Investigations of tip clearance effects in a low speed compressor have been presented by Koch [4] for the Low Speed Research Compressor at the company, General Electric, and by Moyle [5] for measurements made on a 3 stage rig at the Naval Postgraduate School. CFD simulations have also focused on tip clearance effects [6]-[11]. Denton, in a scholarly paper, [12] describes the effect of tip clearance. There has not however been detailed data published for several tip clearance values for high speed test articles operating in the transonic region.

The current study is intended to offer a two-fold research opportunity; direct investigation of the effect of the tip-gap size on the performance of a splittered rotor but also to serve as a useful test case for numerical simulations. In order for the test case to be useful there must be well documented test conditions and an accurate model to perform simulations on. This paper gives the actual inlet conditions, including relative humidity, turbulence intensity, pressures and temperatures that would be required in a flow simulation. The geometry and its manufacture were also tightly controlled and the machined tolerances of the casing were confirmed after manufacture. To vary the tip gap the casing is machined, leaving the rotor geometry unchanged.

Additionally a solid model of the rotor, casing and hub components is available upon request from the authors in a number of solid model formats. The geometry is in the "as machined," cold form and can be used with acknowledgement of this work. This includes complex geometric features such as the mounting bolts and the rotor mounting geometry which some workers may find useful. The geometry also makes

features such as the cavity behind the rotor available for workers interested in simulating secondary flows.

NOMENCLATURE

c_p	Specific heat capacity at constant pressure [J/kg.K]
c_v	Specific heat capacity at constant volume [J/kg.K]
h	Enthalpy [J/kg]
p	Pressure [Pa]
R	Gas constant [J/kg.K]
T	Temperature [K]
M.R.	Mid-range operation
N.S.	Near-stall operation
PR	Stagnation pressure ratio [-]
TR	Stagnation temperature ratio [-]
TG	Tip gap [mm]

Greek Symbols

γ	Specific heat ratio [-]
δ	Ratio of inlet to reference sonic velocity [-]
θ	Ratio of inlet to reference pressure and γ [-]
ρ	Density [kg/m^3]
ω	Humidity ratio [-]

Subscripts

1	Inlet
3	Outlet
a	Air gas
l	Water liquid
mix	Air/water vapor gas mixture
o	Stagnation or dry-bulb
rel	Relative humidity
ref	Standard atmospheric conditions
sat	Saturated wet bulb temperature
v	Water vapor

THE SPLITTERED ROTOR

The test article in use for this work is the result a larger program to develop a design method and test program to investigate novel rotor geometries in a short time frame at relatively low costs. The design method is outlined by Hobson et al [13] with details outlined by Drayton [14]. These works in turn are based on the design methodology outlined by Sanger [15].
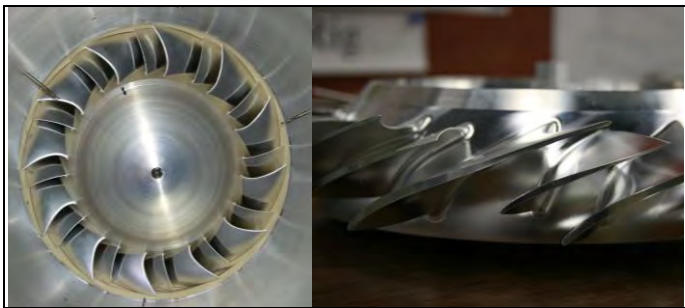

Figure 1. Splittered Rotor.

Figure 1 shows the installed splittered rotor and a close up view of the main and splitter blades. The main features to note are the fact that the splitter blade is fairly far forward compared to some other designs. This leads to it being in the relative supersonic part of the flow. This configuration was found to be more efficient than the traditional method of having the splitter blade reside in the relative subsonic portion of the flow as it results in two weaker oblique shocks.
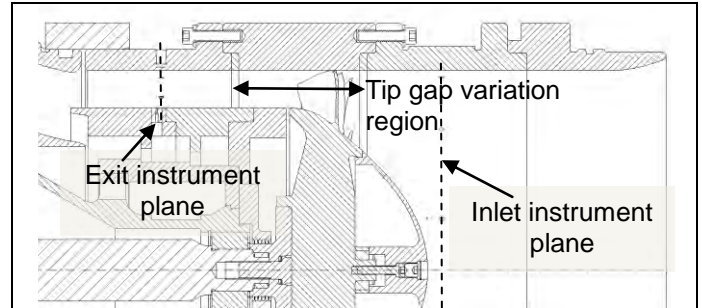

Figure 2. Cross section of rig.

Figure 2 shows the cross-section of the splittered rotor installed within the test rig. The 'Tip gap variation,' region shows the part of the rig that is machined to adjust the tip gap. The casing upstream and downstream of this maintains a constant diameter (see Table 3 for dimensions). Also visible is the large fluid cavity behind the rotor. No attempt was made to capture this region and its effect in the design process but it is expected that there will be inflow and outflow into this cavity across the blade passage. The geometric solid model includes these features and to accurately simulate the flow field seen by the downstream probes this would have to be included.
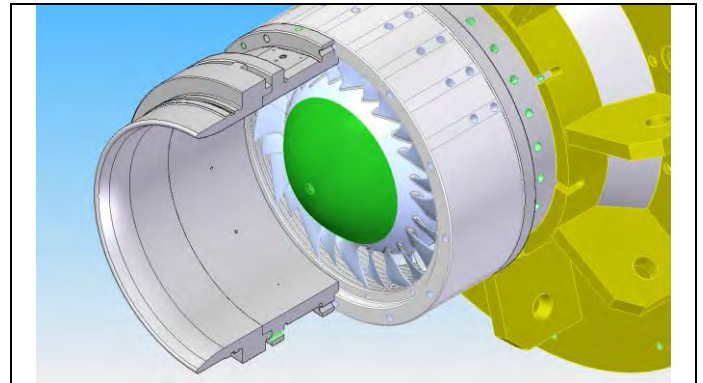

Figure 3. Solid model of rotor and rig.

Figure 3 shows the solid model of the rotor installed in the test rig. The casing, rotor and nose cone are made from 7075-T6 aluminum. While the high strength is not required for the casing it machines more easily and allows more accurate parts to be made. This geometry is available for export in a number of different electronic formats.

Table 1 gives the following properties of the rotor; the constant outer diameter, the inlet diameter of the main blade root and the design speed based on the nominal operating speed of the test rig.

Table 1. Rotor properties

Description	Value
Rotor Diameter [mm] (in)	287.02 (11.300)
Inlet Diameter [mm] (in)	190.70 (7.508)
100% Speed [rpm]	27 000
Total Blade Number [-]	24 (12 Main + 12 Splitter)
100% Tip Speed [m/s]	405.8

Table 2. Main blade and splitter blade properties

Description	Main	Splitter
Tip Chord [mm] (in)	96.60 (3.80)	58.54 (2.30)
Inlet Height [mm] (in)	48.14 (1.90)	46.80 (1.84)
Outlet Height [mm] (in)	28.32 (1.11)	27.94 (1.10)
Blade Number [-]	12	12

Table 2 gives overall dimensions of the main and splitter blades of the rotor at their leading and trailing edges. The chords given are the linear distances from the leading edges to the trailing edges of the blades. The mean of the four blade heights given are used to calculate the ratio of tip-gap to blade height in Table 3.

Table 3. Cold rotor, casing and tip gap sizes

Cold Tip Gap [mm] (in)	0.99 (0.039)	0.76 (0.030)	0.53 (0.021)
Inlet/Outlet Diam [mm] (in)	287.22 (11.308)	Same	Same
Casing Diam. [mm] (in)	289.02 (11.378)	288.54 (11.360)	288.09 (11.342)
Rotor Diam. [mm] (in)	287.02 (11.300)	Same	Same
Tip Gap/Blade Height [%]	2.6%	2.01%	1.40%
Tip Gap/Blade Chord [%]	1.28%	0.98%	0.68%

Table 3 shows the final manufactured dimensions used for the three test cases. The absolute cold tip gaps used are 0.99 mm, 0.76 mm and 0.53 mm and are used as the reference values through this study. As can be seen the rotor diameter does not change while the casing diameter is machined to the desired diameter. Figure 2 shows the region of the casing that is machined while the upstream and downstream casing diameters remain constant. The ratio of tip gap to blade height reflects the mean inlet and outlet blade heights of both the splitter and main blades shown in Table 2. The ratio tip gap to blade chord reflects the mean chord of the main and splitter blades (Table 2).

EXPERIMENT

The transonic compressor rig used here has been described in some detail in previous papers with the current instrumentation configuration and data reduction methods outlined in Hobson et al [16].
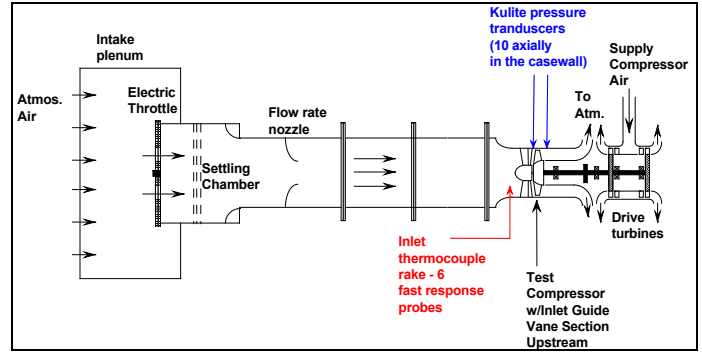

Figure 4. Layout of Transonic Compressor Rig [16].

Figure 4 shows a schematic of the rig with the opposing air driven turbines and upstream throttling configuration. The rig is designed to be adaptable to differing rotor and stator geometries with minor modifications to instrumentation to test a new rotor. The mass flow is measured upstream of the rotor using a calibrated orifice nozzle. Inlet conditions are measured with two combination stagnation temperature and pressure probes. Downstream temperature and pressure profiles are measured with 10 and 20 Kiel stagnation probes respectively. The radial location of the probes is shown in the results of Figure 16 and Figure 17. The location of the upstream and downstream instrumentation holes is shown in Figure 2.

Tip Gap Variation Method

The tip gap in this study is varied by changing the diameter of the outer casing while keeping the diameter of the rotor constant resulting in a constant tip gap around the circumference of the rotor. The process that has been developed to achieve this accurately is outlined.
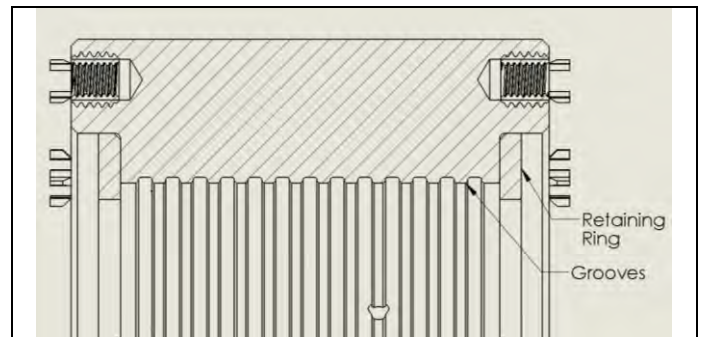

Figure 5. Pre-machined casing geometry.

Figure 5 shows the section geometry of the aluminum casing that is stationed over the rotor. Grooves are machined into the casing to give the abradable material a good purchase surface. Removable oversized retaining rings are then screwed into place on either side of the grooved section. These are sacrificial so that if the process of laying up the abradable material is not successful they can be removed and simply replaced. The casing and rings are machined together and they are left in place and form part of the casing during the experimental testing.
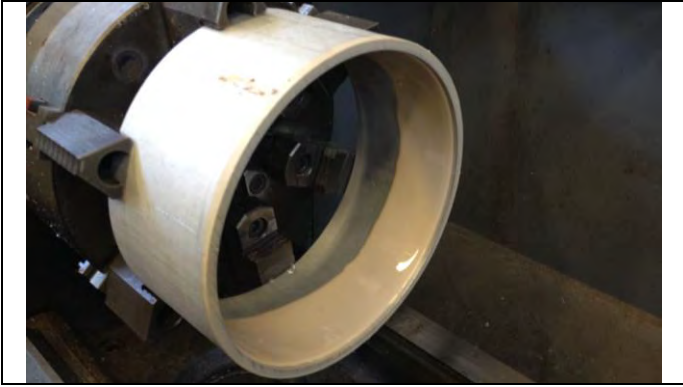
3   Copyright © 2015 by ASME

Figure 6. Curing process of abradable material.

Figure 6 shows the abradable material being spun into place using a lathe. The part shown is a test ring with a representative groove machined out of it. A rotational velocity is used to give one-gravity acceleration to the material when upside down to ensure that no running of the material takes place while setting. A West Systems™ 105 epoxy with a 410 Microlight™ filler is used as this is stiff while being easily machinable and able to hold very tight tolerances. A heat lamp, not shown in the figure is shone onto the part during rotation and improves the curing rate of the material. After an approximately 8 hour rotation the part is left for an additional 2 days to allow the final curing of the epoxy to take place. A noticeable stiffening of the material takes place during this phase. The inner diameter of the retaining ring shown in Figure 5 prior to machining is approximately 5 mm smaller than the final desired size providing a dam or reserve diameter of abradable material. Once the material is properly set the casing is accurately clocked into a lathe and machined to within 50 μm of the desired diameter over its entire length. Once the machined part is removed from the lathe its actual diameter is measured using a micrometer (Table 3).

Figure 7. Machined casing geometry.

Figure 7 shows the final machined casing. Once a set of tests is complete the part is then placed back in the lathe and machined to the next desired diameter. If a smaller diameter is desired the abradable material is sanded out, new retaining rings inserted and the layup and machining process repeated. Once installed over the rotor the casing is adjusted side to side and vertically using shim stock to ensure concentricity to within 12.5 μm (0.0005") using a feeler gage between the rotor blades and casing. The casing upstream and downstream of the rotor ring has a diameter of 287.22 mm (11.308") and forms a backward and forward facing step at the inlet and outlet of the rotor ring respectively. While not ideal this was felt to be the simplest geometry to be used in a test case and the step sizes are of the same order as the inlet boundary layer.

Figure 8. Unsuitable abradable material.

Some experimentation with silicone rubber systems was tried and due to the 'springy' nature of these materials machining them to tight tolerances was difficult. In addition they did not abrade well leading to one rotor failure (Figure 8). It should be noted that an aluminum rotor is used to reduce cost. For the current rotor, three aluminum rotors could be manufactured for the price of a single titanium one. Thus even with the one rotor failure the material choice was cost effective. The silicone materials may be more suited to titanium rotors but investigating this was beyond the scope of this work.

It must be noted that at the speeds being tested rotor deformation or the so-called 'hot' shape geometry does affect the tip gap significantly. A very simple mechanical deflection analysis was performed using the software package "Ansys Mechancial" to obtain radial deformation of the tips of the blades at 27 000 rpm [17].
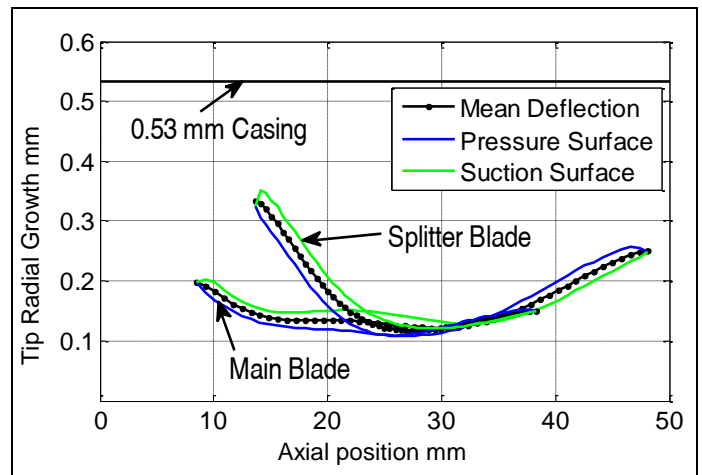

Figure 9. 100% speed radial blade growth.

Figure 9 show the radial growth of the main and splitter blades respectively. The zero position on the y-axis is the un-deformed or cold blade-tip position. Also plotted is the 0.53 mm casing position corresponding to the smallest tip gap. It can

be clearly seen that the variation in the gap is not constant. In the case of the main blade the leading and trailing edges have the largest deflections due to the longer chord at the casing. In the case of the splitter blade the stacking method used leads to the largest overall radial deformation at the blade leading edge.

Table 4 lists the approximate hot tip gaps compared to the cold ones. It can be seen that as a fraction, the decrease in gap is significant. This gap is calculated using the median values of blade growth of the main and splitter blades taken from Figure 9. The average of these two medians is then used to calculate the approximate hot tip gap.

Table 4. Deformed (hot) tip gap sizes

Cold Tip Gap [mm] (in)	0.99 (0.039)	0.76 (0.030)	0.53 (0.021)
Approx. Hot Tip Gap [mm] (in)	0.79 (0.031)	0.56 (0.022)	0.33 (0.013)
Average Median Growth [mm] (in)	0.20 (0.008)	Same	Same
Main blade median growth [mm] (in)	0.18 (0.007)	Same	Same
Splitter blade median growth [mm] (in)	0.23 (0.009)	Same	Same

Air-Water Vapor Mixture Gas Properties

To be an effective test case the inlet properties must be accurately known and this requires taking the relative humidity into account. It has about a 0.5% effect on the specific heat capacity c_p compared to dry air. The method for calculating the gas properties is taken from Borgnakke [18]. The first step in this is to measure the dry bulb, T_{o1}, and wet bulb, T_{sat}, temperatures. T_{o1} is measured at the inlet to the compressor using a stagnation temperature probe while the wet bulb temperature is measured using a sling psychrometer before and after each test.

The saturated vapor pressure of water is only a function of T_{sat} and is obtained using the Matlab™ code X-Steam [20] which is based on the IF-97 standard [21],

$$p_{vsat} = f(T_{sat}) \tag{1}$$

The saturated humidity ratio ω_{sat} is calculated using the ratio of gas constants of air, R_a and water, R_v and the vapor pressure p_{vsat} and compressor inlet stagnation pressure p_{o1} using the following relationship,

$$\omega_{sat} = \frac{R_a}{R_v}\left(\frac{p_{vsat}}{p_{o1} - p_{vsat}}\right) \tag{2}$$

Using ω_{sat} the relative humidity ratio ω_{rel} is calculated using the following thermodynamic relationship,

$$\omega_{rel} = c_{p_a}(T_{sat} - T_{o1}) + \omega_{sat}\left(\frac{h_{vsat} - h_{lsat}}{h_{o1sat} - h_{lsat}}\right) \tag{3}$$

The partial pressure of the water vapor p_v is then,

$$p_v = \frac{\omega_{rel}p_{o1}}{(R_a/R_v) + \omega_{rel}} \tag{4}$$

The specific heat capacity at constant pressure, $c_{p\,v}$ of the water vapor is a function of both the water vapor pressure p_v and inlet temperature T_{o1}. This is due to the fact that the tests were not carried out at saturated atmospheric conditions. X-Steam [20] was used to find the value of $c_{p\,v}$,

$$c_{p_v} = f(p_v, T_{o1}) \tag{5}$$

The specific heat capacity at constant pressure of the air and water vapor mixture, $c_{p\,mix}$ can then be calculated as follows,

$$c_{p_{mix}} = \frac{c_{p_{air}} + \omega_{rel}c_{p_v}}{1 + \omega_{rel}} \tag{6}$$

In the same way the gas constant of the mixture R_{mix} can be calculated,

$$R_{mix} = \frac{R_{air} + \omega_{rel}R_v}{1 + \omega_{rel}} \tag{7}$$

The specific heat ratio at a constant volume c_{vmix} and the specific heat ratio of the mixture, γ_{mix} can then be calculated,

$$c_{vmix} = c_{p_{mix}} - R_{mix} \quad and \quad \gamma_{mix} = \frac{c_{p_{mix}}}{c_{vmix}} \tag{8}$$

The relative humidity, ϕ is not required for the calculations but is a commonly used metric. It is defined as the ratio of the partial water vapor pressure p_v and the saturated water vapor pressure $p_{v\,sat\,01}$ at T_{o1},

$$p_{vsat_{o1}} = f(T_{o1})$$

$$\phi = \frac{p_v}{p_{vsat_{o1}}} \tag{9}$$

As an aside it should be noted that due to the upstream throttling of the rig used the partial pressure p_v entering the compressor decreases while the quantity $p_{v\,sat\,01}$ is only dependent on temperature. This means that the relative humidity of the air entering the compressor is low but the gas mixture properties are not affected as they pass through the throttle.

Scaling Laws

Once the correct gas properties are known then scaling laws can be applied to the results to refer the results to standard atmospheric conditions. The following two scaling constants, θ and δ are used to correct the conditions at the inlet to the rotor to these standard atmospheric values [22],

$$\delta = \frac{P_{o1}\gamma_{mix}}{P_{ref}\gamma_{ref}} \quad and \quad \theta = \frac{\gamma_{mix}R_{mix}T_{o1}}{\gamma_{ref}R_{ref}T_{ref}} \tag{10}$$

The Standard international metric conditions P_{ref} and T_{ref} 101325 Pa and 288.15 K were used respectively [23]. If atmospheric conditions were at standard conditions, then both δ

Copyright © 2015 by ASME

and θ would be unity. Air ideal gas properties for γ_{ref} and R_{ref} of 1.40 and 287 J/kg.K assuming air as an ideal gas at 25°C and 100 000 Pa were used respectively [18]. c_{pref} is then 1004 J/kg.K.

When running the experiment the value θ from eq. (10) is used to ensure that the rotor runs at the correct tip Mach number using the following relationship [22],

$$RPM_{ref} = \frac{RPM}{\sqrt{\theta}} \qquad (11)$$

RESULTS

A range of results is given with the intention of them being useful when compared to numerical simulations and being representative of a wide range of operating conditions. The first results details the inlet gas properties and turbulence intensities. In the second results section performance maps for a wide range of speed-lines and tips gaps are shown. In the third section selected exit profiles of pressure and temperature ratio for two operating points are presented. The first operating point would represent a typical steady-state condition near the mid-range of the compressor operation (M.R.). The second is the near-stall point (N.S.) and the last stable operating point found before stall.

Inlet Conditions

Table 5. Inlet properties at 100% mid-range (M.R.) operation

Tip Gap [mm]	0.99	0.76	0.53
PR [-]	1.69	1.76	1.86
p_{o1} [Pa]	72383	69569	66736
T_{o1} [K]	294.2	290.3	289.9
ρ_{o1} [kg/m^3]	0.853	0.832	0.799
$c_{p\,mix1}$ [J/kg.K]	1010.8	1010.3	1010.6
γ_{mix1} [-]	1.399	1.399	1.399
R_{mix1} [J/kg.K]	288.3	288.1	288.2
δ [-]	0.714	0.686	0.658
θ [-]	1.025	1.015	1.009

Table 6. Inlet properties at 100% near-stall (N.S.) operation

Tip Gap [mm]	0.99	0.76	0.53
PR [-]	1.70	1.81	1.99
p_{o1} [Pa]	71155	67385	63184
T_{o1} [K]	295.7	291.6	289.8
ρ_{o1} [kg/m^3]	0.835	0.802	0.756
$c_{p\,mix1}$ [J/kg.K]	1010.3	1009.8	1010.6
γ_{mix1} [-]	1.399	1.399	1.399
R_{mix1} [J/kg.K]	288.2	288.1	288.2
δ [-]	0.702	0.665	0.623
θ [-]	1.029	1.015	1.009

Inlet properties for the mid-range and near-stall points as indicated on Figure 11 are given in Table 5 and Table 6. These values are calculated using the experimental measurements and the techniques described in the previous section. It is hoped that the use of these will remove some of the uncertainty of numerical simulations. The use of the correct gas properties will affect compressible calculations. The inlet pressures and densities will affect the Reynolds numbers and possibly be important in turbulence models that contain laminar to turbulent transition models. In both sets of tabulated data the greatest deviation from standard inlet conditions is due to the inlet pressure which is reflected in the lower values of δ. While close to unity the values of θ cannot be ignored as their variation from unity is between 0.9% - 2.9%.

Table 5 shows the inlet properties for mid-range operation, assumed to be where the rotor would spend the most operational time. The most notable deviations from standard atmospheric conditions are the inlet pressure, p_{o1} and density, ρ_{01} which are far lower due to the upstream throttling of the compressor rig. This in turn leads to values of δ less than unity.

Table 6 shows the inlet properties for near-stall operation and many of the same trends found in Table 5 are observed. The inlet pressures and densities are lower at the higher operating pressure ratios due the fact that the rig exhausts to atmospheric pressure.
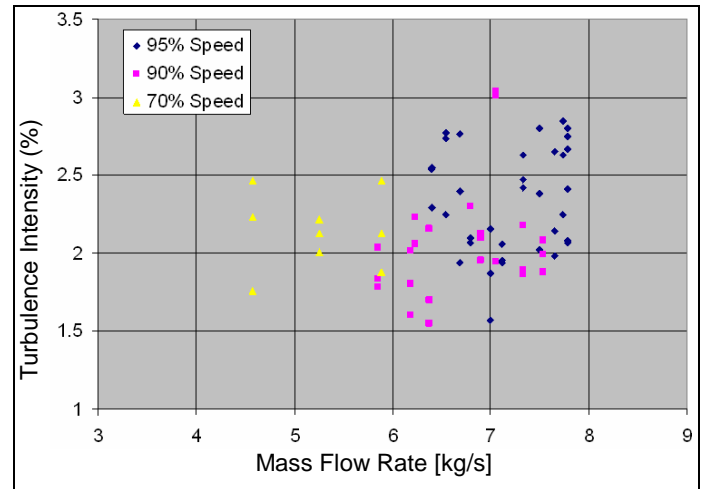

Figure 10. Rig inlet turbulence intensity.

Figure 10 shows the turbulence intensity of the rig inlet as measured by Payne [19] against the mass flow. A TSI 1212-20 20 μm hotfilm probe was used. This was measured for a different rotor, so the speed lines do not correspond to those in this study but the rig inlet geometry has not been modified. The medium turbulence intensity is near 2.25%. The inlet mass flow is accurate and measured at two locations to ensure that no leakage takes place.

Performance Maps

A wide range of operation was tested in the current program. As noted previously the intention is to provide a data

set that is representative of differing compressor stages within a gas-turbine engine.

Table 7. Rotor tip speeds and Mach numbers tested

Speed-line [%]	60	70	80	90	95	100
Tip-speed [m/s]	243.5	284.0	324.6	365.2	385.5	405.8
Tip-Mach [-]	0.71	0.83	0.95	1.07	1.13	1.19

Table 7 gives values of the tip speed and Mach numbers tested. The front stages usually have a smaller ratio of tip-gap to blade height than the aft core stages. In addition the front stages are usually operating in the transonic regime while the rear stages operate sub-sonically due to the temperature gain through the compressor stages.
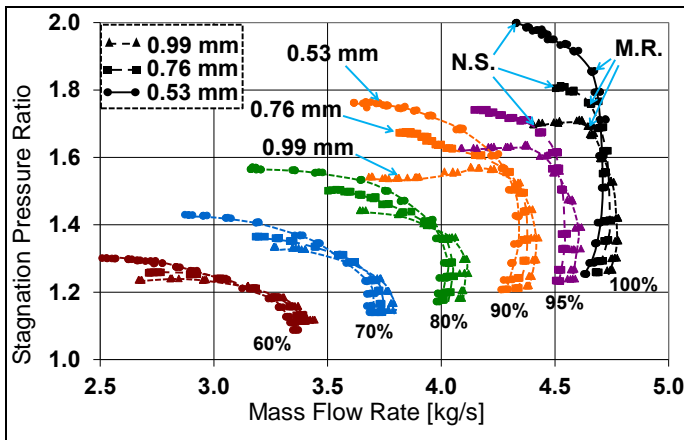

Figure 11. Stagnation pressure ratios.

Figure 11 shows the stagnation pressure ratios for varying tip gaps from subsonic to transonic operation with the corresponding tip Mach numbers and speeds shown in Table 7. Once the relative velocities are taken into account, 80% speed is near sonic at the tip while the rest are firmly supersonic. The transonic test rig in use for this study has an efficient diffuser which allows testing of the chocked flow region with its typical vertical characteristic when operating in the transonic region. These results are left in the main performance maps for completeness but may not be in the typical operating range of a compressor.

Full Open Throttle Operation

As mentioned this mode of operation would not be commonly encountered in an operation engine due to the low efficiency operation at these setting as can be seen in Figure 11 and Figure 12. However due to the interesting flow phenomena and the potential to improve simulations by being able to capture this characteristic it is discussed here. For the full open throttle operation it can be seen that the mass flow rate is higher for the larger tip gaps for all speeds lines. This is to be expected as the effective area of the fan passage has been increased.

When the pressure ratio is low, flow is entrained in the tip gap thereby increasing the overall mass flow rate. As the throttle on the experimental rig is closed and the compressor moves up a speed-line a crossover point occurs and the mass flow decreases with increasing tip gap due to leakage flow through the tip gap. At 60% and 70% speeds the slope the speed-line is unremarkable with the mass flow decreasing with increasing pressure ratio.
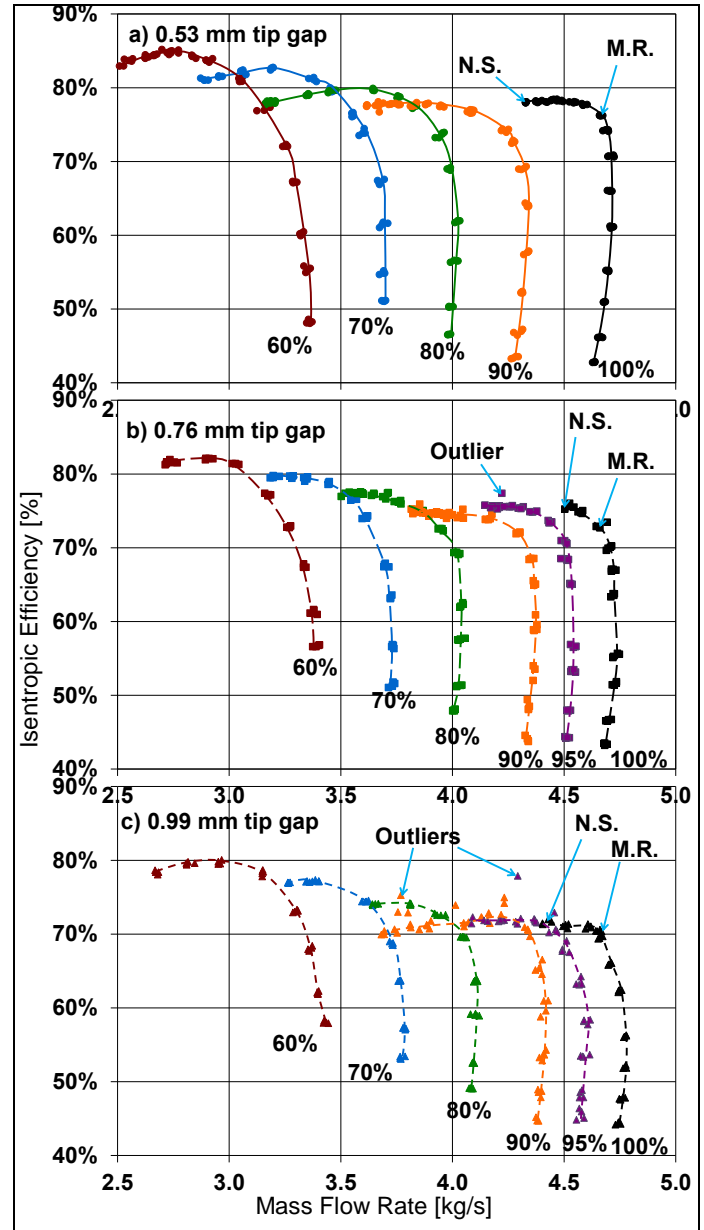

Figure 12. Isentropic efficiencies.

For 80% speed and above the speed-lines become less conventional; the mass flow initially increases with increasing pressure ratio. This was initially predicted during the design phase and at that stage considered to be an error in the simulation [14] however the experimental results showed that

the predictions were correct. While it is beyond the scope of this study to discuss this in detail it appears to be due to the changing shock structure as the pressure ratio increases. This explains why for the subsonic cases it does not appear. Also recall that the flow through the blade is supersonic at low pressure ratios with the final normal shock being at the trailing edge of the blade meaning there is not sonic throat within the blade passages. The absolute efficiencies for the open throttle operation are extremely low as shown in Figure 12.

Mid-Range to Near-Stall Operation

The mid-range (M.R.) operation points and region are marked on Figure 11 and Figure 12 for 100% speed. The mid-range points were chosen based on their efficiency values being the first point where the compressor begins to operate along a traditional operating line with mass flow decreasing as the pressure ratio increases. It is postulated that with the splittered design the rotor may appear to behave as two separate systems. This postulation would appear to be correct in observing the behavior of the operating lines in the transonic region. They initially are very vertical and then at around the mid-range operating region begin to behave in a more traditional way with the mass flow decreasing as the pressure ratio increases. The design process focused on improving the mid-range to near-stall operation leading to this type of behavior [14]. The shock structure's movement from the rear to the front of the rotor during throttling in a splittered rotor is more complex than for a standard single blade-type rotor.

In Figure 11 the effect of a larger tip gap can be seen by the reduction of the stalling pressure ratio when operating above the mid-range point. For the very large tip gap of 0.99 mm the near stall pressure ratio is actually decreases towards stall for the 90%-100% speed-lines. Figure 12 shows that the efficiencies decrease significantly for increasing tip gaps in all cases.

Near-Stall Operation

The near-stall (N.S.) operating points are the last stable operating points before a very small closing of the throttle caused the compressor to stall. Some interesting differences are observed in the behavior of the compressor near to stall for the differing tip gaps.

The largest operating range is found for the smallest 0.53 mm tip-gap case. At 100% speed a 1.99 stagnation pressure ratio is the highest measured for this rotor. For this small tip-gap case the stall occurred immediately after a final small movement of the throttle and it was thus simple to determine the operating range.

For the larger 0.76 mm tip gap the range of operation is smaller as is usually expected and is true across all speed-lines. Some instability was observed during the 95% operation near to stall as can be seen in the single outlier point in Figure 12b. For the two larger tip-gaps when operating near to stall, a short unexpected single surge cycles into and out of stall occurs. Sampling sometimes takes place during these events and as the temperature and pressure measurements are sampled

sequentially erroneous performance values are calculated. They are left in the figures as measured for completeness.

For the very large tip-gap case shown in Figure 12c many more of these outlier points can be seen. In Figure 11 it can be seen that for the 90%-100% speed-lines the operating range is wider which was unexpected. In the 90% case no stall actually occurred during testing as a loud single note harmonic was heard from the compressor. This increases markedly in volume as the throttle is closed and so a decision was made not to operate the compressor in this condition for fear of damaging the rotor. For the 95% and 100% cases the short single stalls were more prevalent which leads to difficulty in determining the exact last stable operating point.
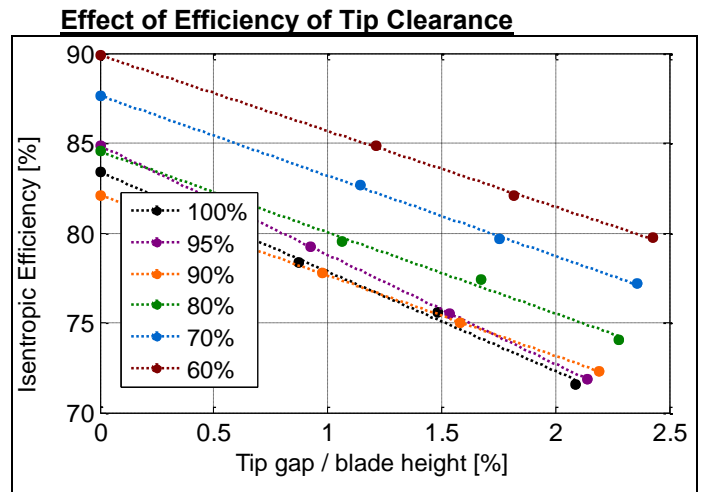
Effect of Efficiency of Tip Clearance

Figure 13. Maximum efficiencies as a function of tip gap.

An investigation of the effect of the tip gap on the efficiency is now undertaken. Figure 13 shows the absolute value of the maximum efficiency measured against the non-dimensionalized tip gap. The tip gap to blade height ratios were calculated using the data from Table 4. For the tip gaps at lower speeds the usual quadratic relationship between deflection and rotor speed was used. The zero tip-gap case is extrapolated from the speed line data using a linear function. The use of a higher order polynomial with only three data points was not considered prudent. As can be seen the overall trend is similar across the speed-lines.
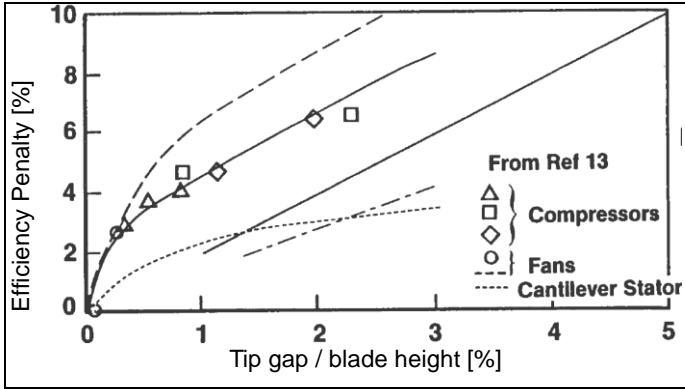
Figure 14. Efficiency penalties, Wisler [3].

Figure 14 presents data from Wisler [3] based on experimental measurements. It shows the expected decrease in efficiency versus the non-dimensionalized tip gap. According to this work, fans appear to be more sensitive to the tip gap than compressors. It must be noted that the x-axis for this figure covers a wider range of tip-gap heights than in Figure 13 and Figure 15.
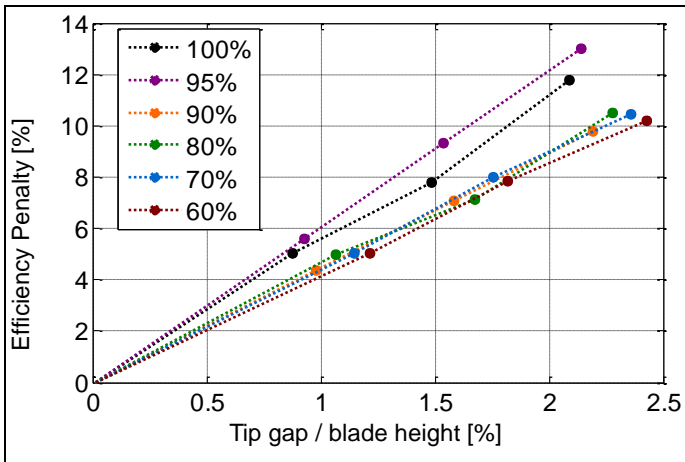

Figure 15. Efficiency penalties for splittered rotor.

Figure 15 shows the same type of data as that from Figure 14 but for the current splittered rotor. Comparing the data set to that of Wisler [3] it can be seen that the splittered rotor has the steeper penalty curve characteristic of a fan. For the range of tip gaps investigated however no leveling out of the penalty curve was seen with the lines appearing to be linear until some further point. Looking at the data from the splittered rotor it can be seen that there is a good correlation in the penalties from 60% to 90% speed. At 95% and 100% speeds steeper curves are found. This is presumably an effect of the stronger shocks that are present due to the supersonic flow.

Exit Profiles

Figure 16 shows the exit stagnation pressure ratio profiles for the three tip gaps tested for mid-range (a) and near-stall (b) operation. Data points are located at the location of the downstream stagnation pressure and temperature probes. The

overall pressure ratios increase with decreasing tip gaps with a noticeable increase in the pressure ratio at the blade tip for the smallest gap for both cases. In Figure 16 b) for the near-stall case the influence of the tip gap is large with a significant increase in the pressure ratio. This indicates that the rotor tip is the location of the stall.
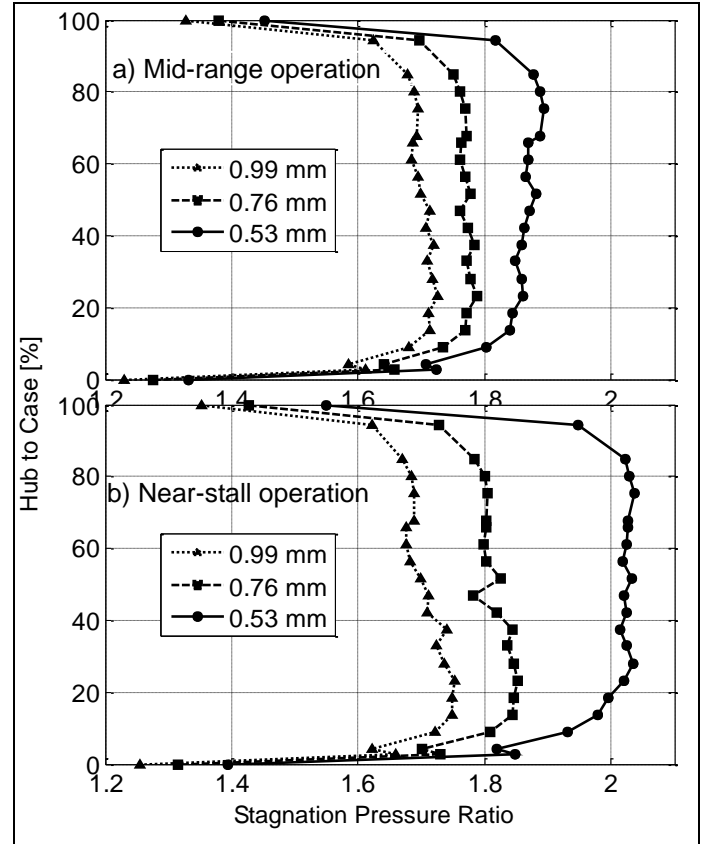

Figure 16. 100% speed stagnation pressure ratio profiles.

Figure 17 shows the exit stagnation temperature ratio profiles for the three tip gaps tested for mid-range (a) and near-stall (b) operation. Again the data points reflect the position of the stagnation temperature probes.

As with the pressure ratio's profiles there is a similar trend of increasing temperature ratios with decreasing tip gaps. While there is less resolution in the data due to fewer temperature probes being used a marked increase in the temperature ratio downstream of the blade tips can be seen. As expected there is an increase in the temperature ratio as stall is approached.
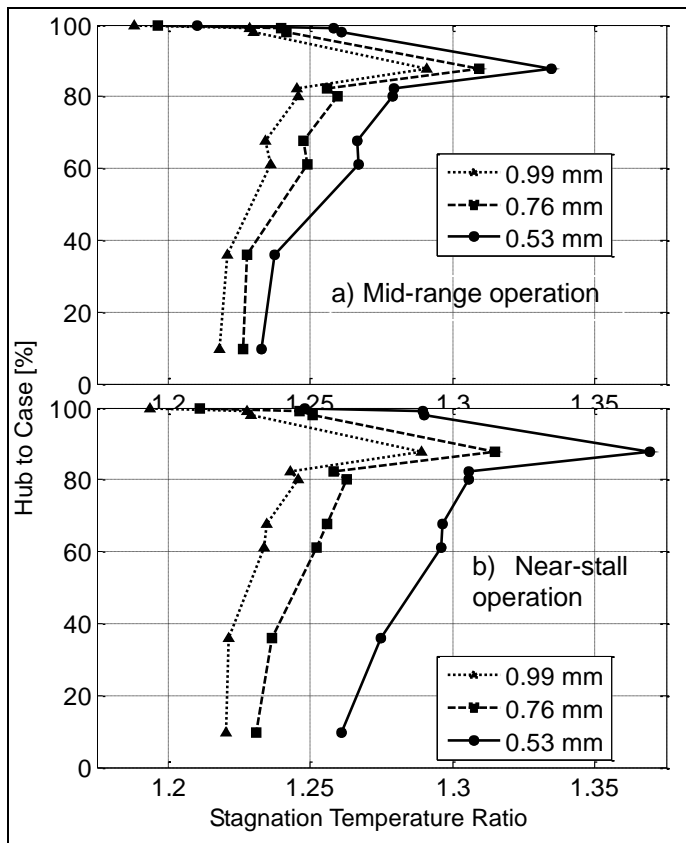
Figure 17. 100% speed stagnation temperature ratio profiles.

CONCLUSION

The first completed experimental test of a splittered transonic compressor rotor as part of a program to test novel geometries has been completed. In the experiments presented here, three different tip gaps were tested and three sets of data obtained. The test were completed over a wide speed range and this coupled with the varying tip gaps means that the data is applicable to transonic front stages with small tip gap to blade height ratios and also to subsonic core stages with larger tip gap to blade height ratios. Non-dimensionalized effects of the increase of the tip gap on the efficiency are presented.

The data presents a useable test case as the inlet conditions are well documented. These include the gas mixture properties taking into account water vapor which has a small but measureable effect. Also given are the absolute pressure and temperature at the inlet to the compressor which are important in simulating the correct Reynolds numbers. The geometry is available upon request.

ACKNOWLEDGMENTS

REFERENCES

[1] Cumpsty, N., Compressor Aerodynamics, Longman Scientic and Technical, 1989.

[2] Freeman, C., "Effect of Tip Clearance Flow on Compressor Stability and Engine Performance," *Tip Clearance Effects in Axial Turbomachines,* No. 1985-05 in Lecture Series, von Karman Institute for Fluid Dynamics, April 1985.

[3] Wisler, D.C., "Advanced Compressor and Fan Systems," lecture notes, General Electric Aircraft Engine Business Group, Cincinnati, OH.

[4] Koch, C.C., "Stalling Pressure Rise Capability of Axial Flow Compressor Stages," *Journal of Engineering for Gas Turbines and Power,* Vol. 103, No. 4, 10 1981, pp. 645-656.

[5] Moyle, I.N., *An Experimental and Analytical Study of Tip Clearance Effects in Axial Flow Compressors,* Phd thesis, University of Tasmania, December 1991.

[6] Beheshti, B.H., Teixeira, J.A., Ghorbanian, K., Farhanieh, B., and Ivey, P. C., "Parametric Study of Tip-Clearance Casing-Treatment on Performance and Stability of a Transonic Axial Compressor," *Journal of Turbomachinery,* Vol. 126, No. 4, 12 2004, pp. 527-535.

[7] Furukawa, M., Saiki, K., Nagayoshi, K., Kuroumaru, M., and Inoue, M., "Effects of Stream Surface Inclination on Tip Leakage Flow Fields in Compressor Rotors," *Journal of Turbomachinery,* Vol. 120, No. 4, 10 1998, pp. 683-692.

[8] Sakulkaew, S., Tan, C.S., Donahoo, E., Cornelius, C., and Montgomery, M., "Compressor Efficiency Variation With Rotor Tip Gap From Vanishing to Large Clearance," *Journal of Turbomachinery,* Vol. 135, No. 3, 03 2013, pp. 031030-031030.

[9] Shabbir, A. and Adamczyk, J.J., "Flow Mechanism for Stall Margin Improvement due to Circumferential Casing Grooves on Axial Compressors," *Journal of Turbomachinery,* Vol. 127, No. 4, 03 2004, pp. 708-717.

[10] Sirakov, B.T. and Tan, C.-S., "Effect of Unsteady Stator Wake Rotor Double-Leakage Tip Clearance Flow Interaction on Time-Average Compressor Performance," *Journal of Turbomachinery,* Vol. 125, No. 3, 08 2003, pp. 465-474.

[11] Bruna, D. and Turner, M.G., "Isothermal Boundary Condition at Casing Applied to the Rotor 37 Transonic Axial Flow Compressor," *Journal of Turbomachinery,* Vol. 135, No. 3, 03 2013, pp. 034501-034501.

[12] Denton, J.D., "The 1993 IGTI Scholar Lecture: Loss Mechanisms in Turbomachines," *Journal of Turbomachinery,* Vol. 115, No. 4, 10 1993, pp. 621-656.

[13] Hobson, G.V., Gannon, A.J. and Drayton, S., "Design and Test of a Transonic Axial Splittered Rotor," ASME Turbo Expo 2015, Montreal, Canada, Paper No. GT2015-43005.

[14] Drayton, S., "Design, Test, and Evaluation of a Transonic Axial Compressor Rotor with Splitter Blades," PhD thesis, Naval Postgraduate School, Monterey, CA 93943-5000, September 2013.

[15] Sanger, N.L., "Design Methodology for the NPS Transonic Compressor," TPL Technical Note 99-01, Turbopropulsion Laboratory, Naval Postgraduate School, Monterey, CA 93943-5000, August 1999.

[16] Hobson, G.V., Gannon, A.J., Holmes, W., and McCormick, M., "Experimental and Numerical Performance Characterization of a Transonic Compressor Rotor Operating Behind an Inlet-Guide Vane with Variable Flap Angles," ASME Turbo Expo 2014, Dusseldorf, Germany, Paper No. GT2014-27308.

[17] Nemnem, A., Private Communication, Doctoral Student, University of Cincinnati, Aerospace Engineering Dept, 2014.

[18] Borgnakke, C., and Sonntag, R. E., "Fundamentals of Thermodynamics," John Wiley & Sons, Inc, 2009 pp 530-548.

[19] Payne, T.A., "Inlet Flow-Field Measurements of a Transonic Compressor Rotor Prior to and During Steam-Induced Rotating Stall," Master's Thesis, Naval Postgraduate School, 2005.

[20] Holmgren, M., "XSteam.m," Matlab™ file, http://www.mathworks.com/matlabcentral/fileexchange/9817-x-steam--thermodynamic-properties-of-water-and-steam , 2007.

[21] Cooper, J. R. & Dooley, R. B., "Revised Release on the IAPWS Industrial Formulation 1997 for the Thermodynamic Properties of Water and Steam," The International Association for the Properties of Water and Steam Lucerne, Switzerland, August 2007.

[22] Von Backström, T.W., "The Effect of Specific Heat Ratio on the Performance of Compressible Flow Turbo-Machines," ASME Turbo Expo 2008, Berlin, Germany, Paper No. GT2008-50183.

[23] "Natural gas – Standard reference conditions", ISO 13443, International Organization for Standardization, Geneva, Switzerland ISO Standards Catalogue.